Materials and Design 31 (2010) 3442–3448

Contents lists available at ScienceDirect

Materials and Design

journal homepage: www.elsevier.com/locate/matdes

The thermal fatigue resistance of vermicular cast iron coupling with H13 steel units by cast-in process

Chengtao Wang [a,b], Hong Zhou [a,*], Peng Yu Lin [a], Na Sun [a], Qingchun Guo [c], Peng Zhang [a], Jiaxiang Yu [a], Yan Liu [a,d], Mingxing Wang [e], Luquan Ren [f]

[a] The Key Lab of Automobile Materials, The Ministry of Education, Jilin University, Changchun 130025, PR China
[b] Faw–Volkswagen Automotive Company Ltd., Changchun 130011, PR China
[c] Brilliance Automobile Engineering Research Institute, Shenyang 110141, PR China
[d] The Metallurgical Engineering Department, Liaoning Institute of Science and Technology, 42 Wenhua Road, Benxi 117022, PR China
[e] The State Key Laboratory of Nonlinear Mechanics, Institute of Mechanics, Chinese Academy of Sciences, 15 Beisihuanxi Road, Beijing 100190, PR China
[f] The Key Lab of Terrain Machinery Bionics Engineering, The Ministry of Education, Jilin University, Changchun 130025, PR China

ARTICLE INFO

Article history:
Received 13 September 2009
Accepted 22 January 2010
Available online 28 January 2010

Keywords:
Vermicular cast iron
H13 steel
Cast
Bionics
Microstructure
Thermal fatigue resistance

ABSTRACT

This paper focuses on improving the thermal fatigue resistance on the surface of vermicular cast iron coupling with inserted H13 steel blocks that had different cross sections, by cast-in processing. The microstructure of bionic units was examined by scanning electron microscope. Micro-hardness and thermal fatigue resistance of bionic samples with varied cross sections and spacings were investigated, respectively. Results show that a marked metallurgical bonding zone was produced at interface between the inserted H13 steel block and the parent material – a unique feature of the bionic structure in the vermicular cast iron samples. The micro-hardness of the bionic samples has been significantly improved. Thermal resistance of the samples with the circular cross section was the highest and the bionics sample with spacing of 2 mm spacing had a much longer thermal fatigue life, thus resulting in the improvement for the thermal fatigue life of the bionic samples, due to the efficient preclusion for the generation and propagation of crack at the interface of H13 block and the matrix.

1. Introduction

Gray cast iron has been widely used in vehicles as a major material for brake drums, exhaust pipes and cylinders because of its low cost and desirable properties such as low melting point, good fluidity and cast-ability, excellent machinability, better wear resistance and other good properties [1–5]. However, for the brake drums, the alternately heating and cooling caused by frequently braking may bring as a result to initiation and propagation of thermal crack. As a result, the thermal fatigue caused by internal stresses, leads to the initiation and propagation of cracks, as a main reason for the failure of brake drums [6–10], and furthermore, temperature, time, and service environment have significant influence on thermal fatigue resistance as well, particularly in the view that the situation sets higher requirements to obtain braking properties of the braking drum. It is important and urgent to improve and to enhance the frictional wear properties and thermal fatigue resistance of brake drum materials. Improving the mechanical properties of brake materials is mainly done by adding alloy elements [1,11,12]. Mitsubishi Motors has used gray cast iron with 1.2% of nickel, plus chromium and molybdenum added in trucks as the material for brake drums [1]; Cheng et al. [13] found that the microstructure and mechanical properties of cast iron were improved by means of micro-alloying with 0.51% Cu and 0.32% Cr (in wt.%) and reported its improvement for the service life of brake drums. Nevertheless, it is noted that with regarding to the difficulty of choosing suitable elements with proper chemical compositions, it is difficult to enhance the thermal fatigue resistance in this way without sacrificing the mechanic property of the bulk materials.

In the present study, we investigated thermal resistance of vermicular cast iron by cast-in processing coupling inserted H13 steel blocks on the basis of the simulation of the surface structure of shells, with a purpose to probe the mechanisms behind the experimental results.

2. Experimental procedure

2.1. Experimental materials

The matrix was vermicular cast iron, with similar chemical compositions to the material used for brake drums. The inserted

* Corresponding author. Tel.: +86 431 85094427; fax: +86 431 85095592.
E-mail address: wangct08@mails.jlu.edu.cn (H. Zhou).

0261-3069/$ - see front matter Crown Copyright © 2010 Published by Elsevier Ltd. All rights reserved.
doi:10.1016/j.matdes.2010.01.041

Table 1
The chemical composition of experimental materials.

Element	Composition (wt.%)								
	C	Si	Mn	P	S	Cr	M0	V	Fe
Vermicular cast iron	3.6	2.4	0.5	<0.06	<0.06	–	–	–	Balance
H13 steel	0.3–0.5	0.8–1.2	0.2–0.5	⩽0.03	⩽0.03	4.7–5.5	1.1–1.8	0.8–1.2	Balance

Table 2
The specific parameters of H13 biomimetic units.

Shape of the units	Specimen size (mm)	Spacing of units (l/mm)		
Circular	$d = 5$	2	3	5
Square	$a = 4.5$	2	3	5
Rectangle	$a \times b = 6 \times 3.5$	2	3	5

material is H13 hot-worked die steel. Chemical composition of the mentioned-above materials is illustrated in Table 1.

2.2. Sample preparation

The inserted H13 steel units were cut by an electric spark machine (DK 7732), with the specific parameters given in Table 2 and a schematic illustration of bionic samples is shown in Fig. 1. Seventy-two units with the same cross sectional area were divided into three groups and there were eight inserted H13 steel blocks with different spacing in each group. These inserted blocks in each group were located vertically at the bottom of a sand mould. During casting, the vermicular cast iron was melted by a medium-frequency induction furnace, and then poured into a green mould at 1450–1500 °C, solidified with the H13 blocks inside, and then cooling down to room temperature. The samples were cut by the electric spark machine with a gauge section of $85 \times 20 \times 6\,(mm^3)$. In order to be fixed onto the plate of a thermal fatigue experimental machine, a hole of 3 mm in diameter was drilled at one side of each sample. In addition, all the samples were mechanically polished to remove all the surface irregularities and machining marks before a thermal fatigue test.

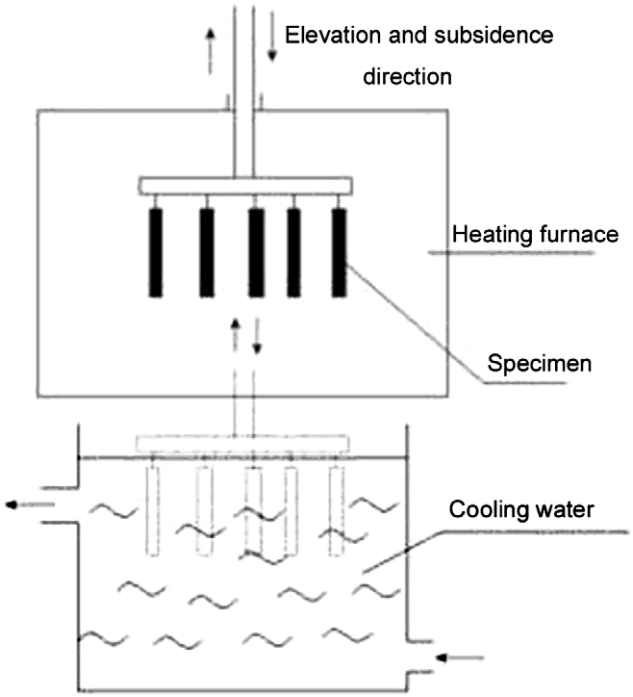

Fig. 2. The sketch of the thermal fatigue tester.

2.3. Experimental methods

After the cast-in processing, a transverse section was obtained from each sample, and standard methods of metallography were

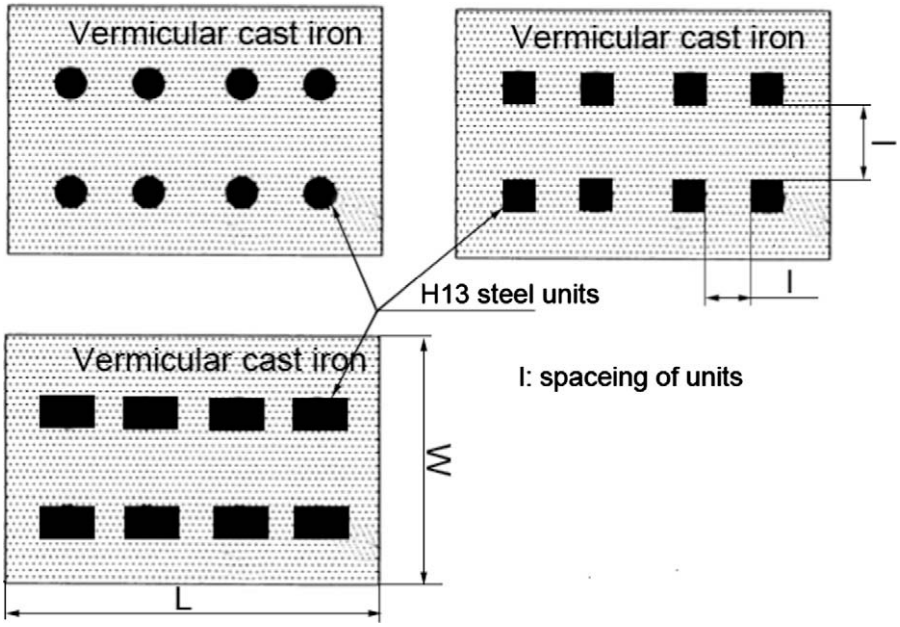

Fig. 1. The schematic illustration of the bionic specimens.

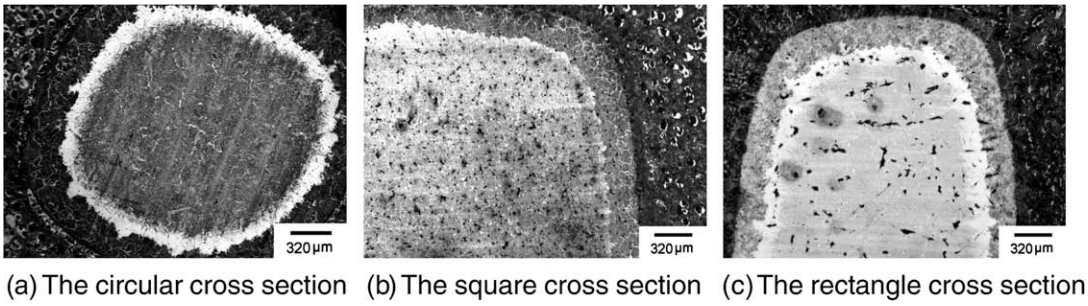

Fig. 3. Bionic units with different cross sections.

followed for microstructure, phase and crack propagation analysis. The 4 vol.% HNO_3–alcohol solution was used to produce the microstructure for observations. An optical microscope and a scanning electron microscope of type (JSM – 5500 LV, Japan) were used for the investigation. The micro-hardness measurements were carried out using a Vickers Micro-hardness Tester (model 5104, manufactured by Buehler Co. Ltd., USA) with a 25 g load.

Thermal fatigue tests were carried out using a self-restraining thermal fatigue tester (as shown in Fig. 2). The samples were heated by a resistance furnace and then cooled by running water. The machine could record thermal cycle times automatically. The furnace temperatures were controlled by silicon control of model (KSY – 12-6), and temperature of the samples was monitored by a thermocouple attached to the sample at center of its length. A complete thermal cycle included heating for 90 s up to 700 ± 5 °C, and then cooled for 3 s to 25 ± 5 °C. The samples were free from any externally applied load, and were taken out to observe the cracks on the surface of samples every 50 cycles. The length of cracks was measured after every 200 cycles, during the fatigue test from 300 and 700 cycles. Finally, the thermal fatigue properties of samples were statistic evaluated.

3. Results and discussion

3.1. Microstructure of bionic samples

The inserted H13 steel blocks with varied cross sections (see Fig. 3) were used during the casting processing. During cast-in, surface area along the inserted H13 steel blocks had been molten, and then solidified, carbon in the matrix had diffused into fused zone along the surface of blocks and led to the formation of graphite and a small amount of ledeburite in the transition zone due to rapid solidification. A transition zone was formed between the matrix and the H13 steel blocks due to the formation of desired metallurgical combination. The bionic sample, as indicated, consists of a transition zone, interface and inserted H13 steel blocks, as shown in Fig. 4. All the inserted blocks exhibit no porosity and few imperfections and a sound metallurgical bonding zone is produced at interface between the inserted H13 steel blocks and the parent material – a unique feature of the bionic structure in the vermicular cast iron samples.

The composition of interface has changed largely, and the major phase of H13 units is martensite with grain boundaries between

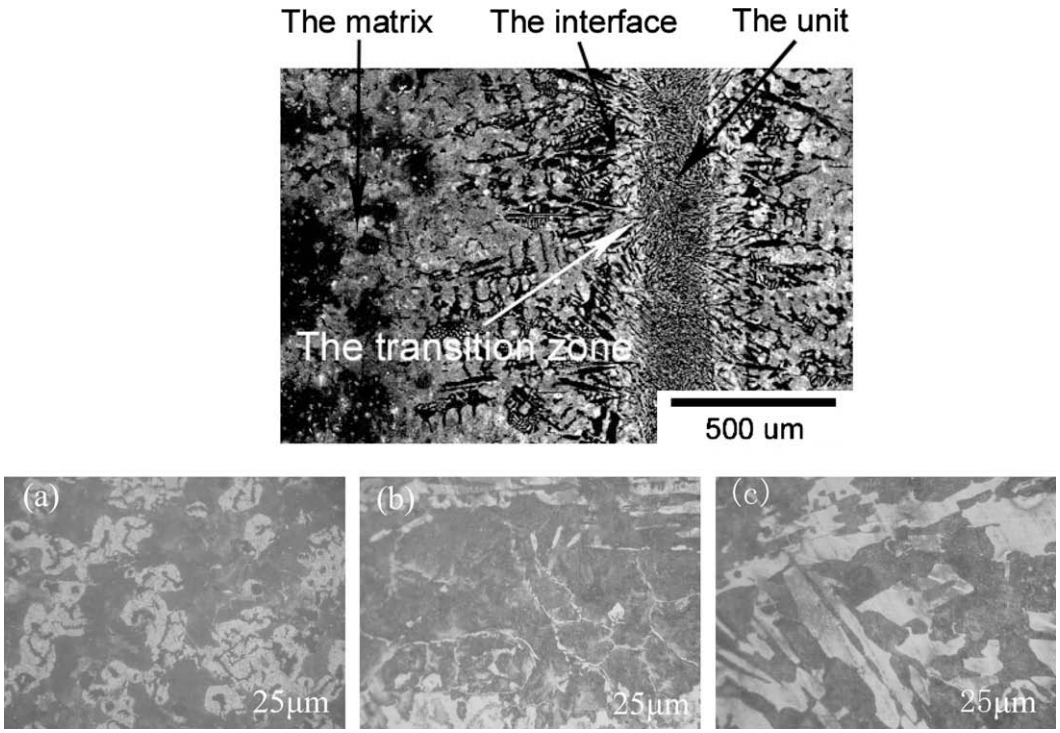

Fig. 4. The microstructure of bionic units.

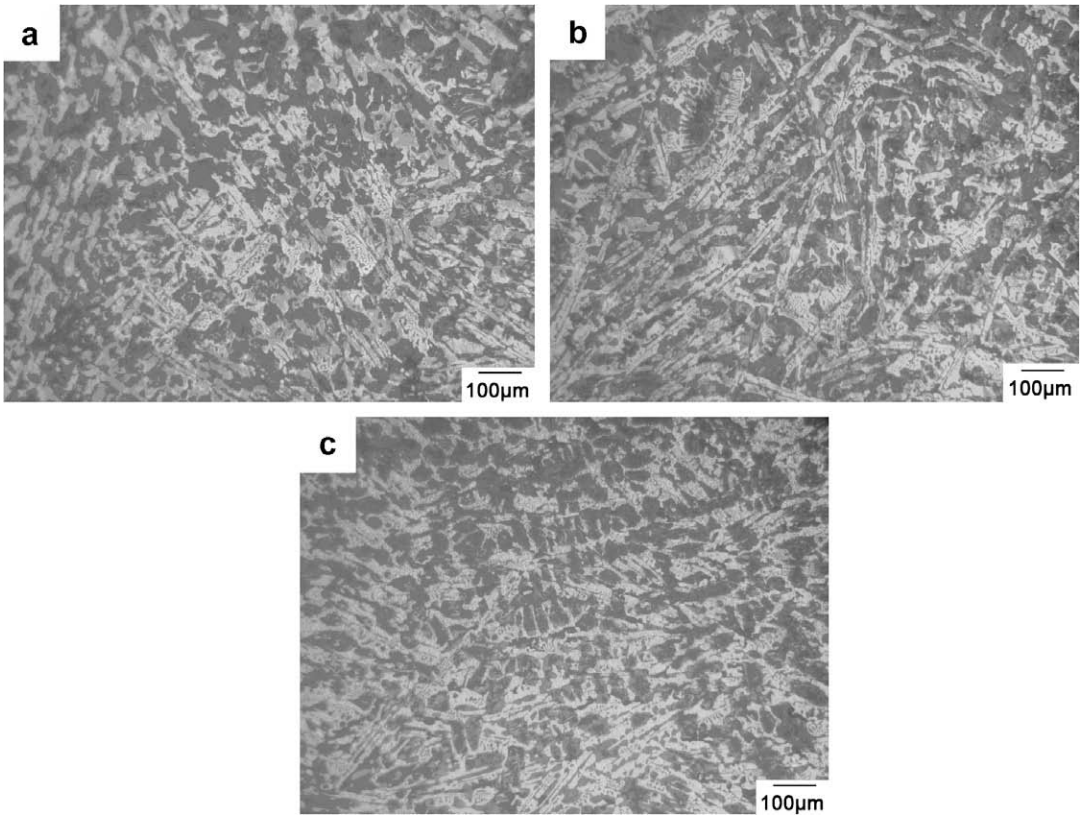

Fig. 5. Microstructures of transition zone with different shape of H13 units: (a) circular, (b) rectangle, and (c) square.

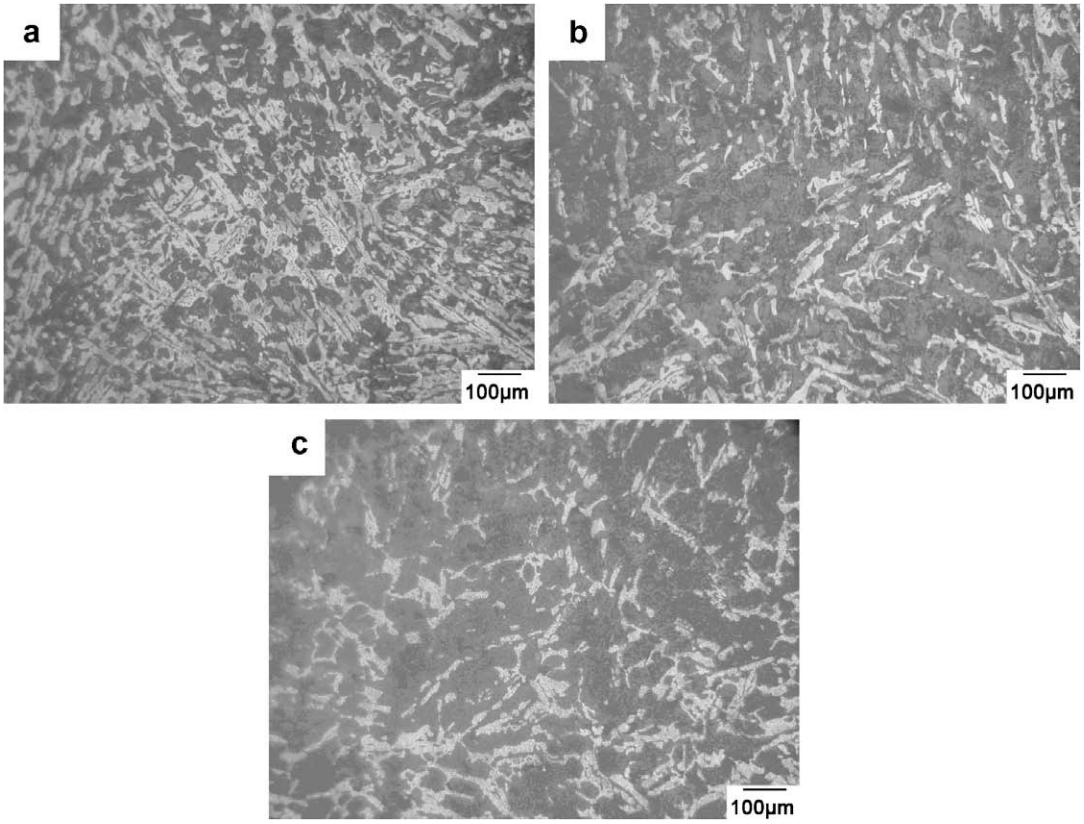

Fig. 6. The microstructure of transition zone with different spacing: (a) 2 mm, (b) 3 mm, and (c) 5 mm.

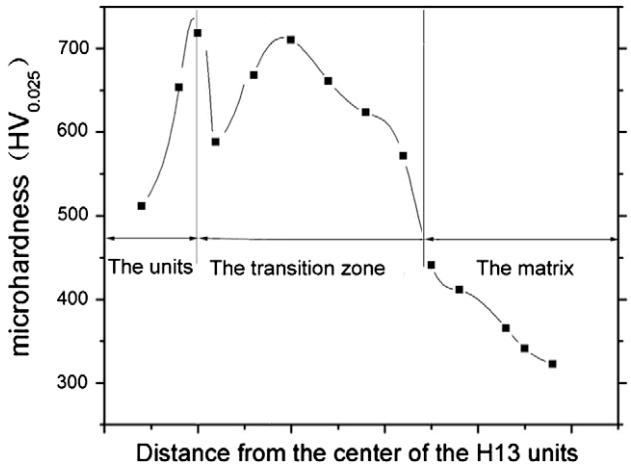

Fig. 7. Micro-hardness vs. distance from the center of units to the matrix after the casting process (error = ±25 HV).

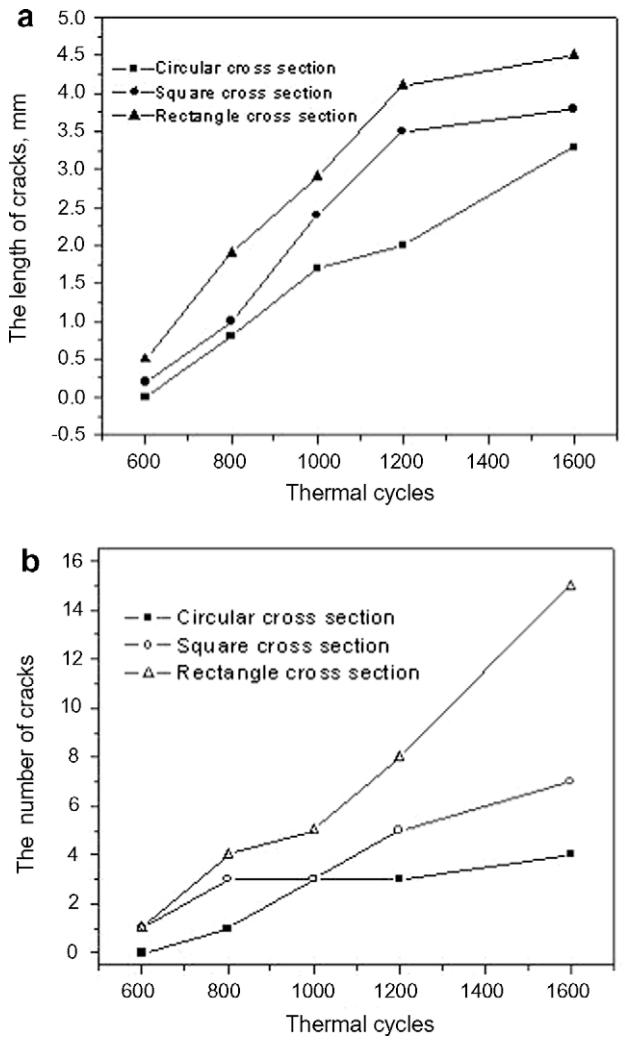

Fig. 8. The length of cracks (a) and the number of cracks (b) as a function of cross section.

columnar crystals. Pearlite and ledeburite eutectic consist the matrix of sample. The transition zone consists of graphite and ledeburite. During solidification, the graphite in the matrix diffused towards the surface, and elemental carbon was released into the

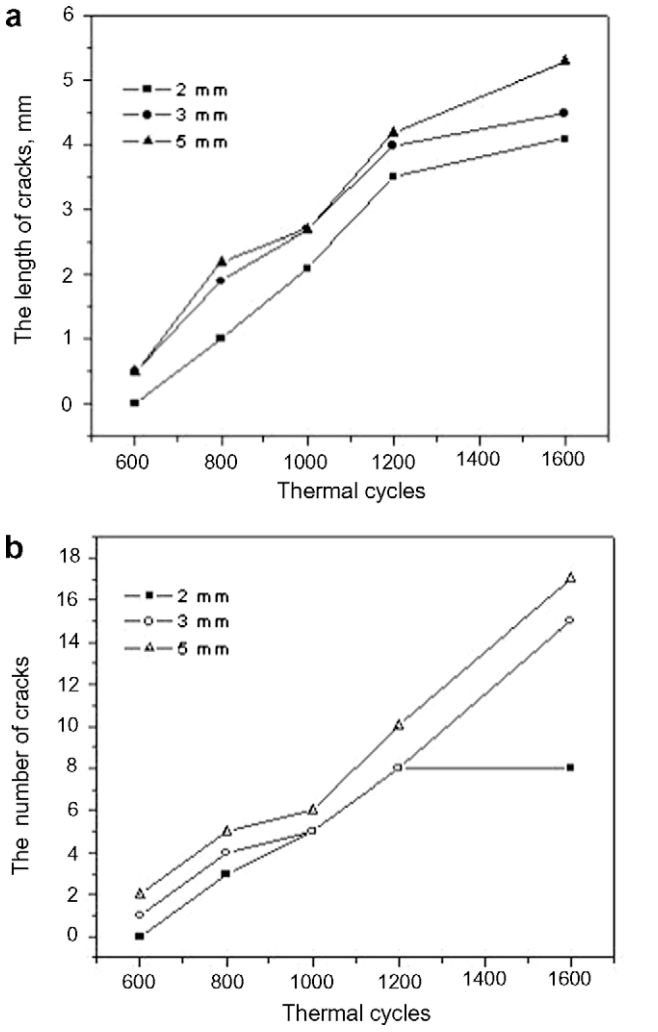

Fig. 9. The length of cracks (a) and the number of cracks (b) as a function of units spacing.

transition zone. The time available for this movement determines the carbon concentration in the transition zone. Austenite precipitates as dendrites, and at the eutectic temperature, the remaining solidifies as ledeburite ($\gamma + Fe_3C$). However, further cooling left no time for graphite to nucleate anymore. In this scenario, the already dissolved graphite nodules may also be present in the solidified surface. An increased proportion of ledeburite is observed, as shown in Fig. 5.

The varied microstructures are determined by the cooling rates of the cast-in processing. Higher cooling rate results in a fine grained microstructure, which may contain non-equilibrium phases, novel precipitates and extended solid solubility in the circular cross section of H13 blocks, and it can make the microstructure much finer. As can be seen form Fig. 6, the amount of ledeburite in the bionic sample with 5 mm spacing is the lowest among all samples examined in the present study, and the amount of ledeburite in the bionic sample with 2 mm spacing is the highest in the transition zone. It can be seen that microstructure in transition zone becomes much finer from Fig. 6a–c.

3.2. Micro-hardness

Fig. 7 shows the dependence of micro-hardness on the distance from the center of the insert blocks to the matrix. It is found that micro-hardness curves of all the bionic samples with different

cross sections and varied spacing measured in the investigation follow the same trend of microstructures. It can be seen that the micro-hardness of transition zone and units are much higher than that of the matrix. In a word, the presence of ledeburite at the surface exhibits a beneficial effect on micro-hardness and hardness at the transition area on the surface is the highest among all the samples, due to its fine microstructures.

3.3. Thermal fatigue resistance

During the fatigue cycles, the length of cracks was measured and then the number was counted at the surface of every sample. Fig. 8 shows the results as a function of the cross section. We can see that the crack on the bionic samples with the circular cross section before 600 periods for fatigue test is almost negligible, which is much better than those thermal specimens processed by laser beam [14,15], but for those with both square and rectangular cross section, the surface demonstrates the presence of some cracks. A main crack in length of 0.8 mm was initially detected on the sample with the circular cross section as the fatigue test reached 800 fatigue periods. In comparison, we found three 1 mm main cracks for the sample with the square cross section and, four 1.7 mm main cracks for the one with rectangle cross section. As the fatigue test progressed, both the length and the number of main cracks increased. After 1600 fatigue periods, three 3.3 mm main cracks were found at the surface of the sample with the circular cross section; for those with square and rectangular cross section, five 3.7 mm main cracks and fifteen 4.3 mm cracks were found, respectively. The crack length increases with the order of rectangle, square, and circular. Meanwhile, the number exhibits the reverse trend: that is, rectangle > square > circular. Therefore, we give the conclusion that the crack propagation resistance of the bionic sample with the circular cross section is the best, then sample with the square cross section. It is also becomes clear from these results that the crack propagation rates of samples processed by cast-in are much better than those by laser beam [16], due to the sound metallurgical bond and lower stress concentration.

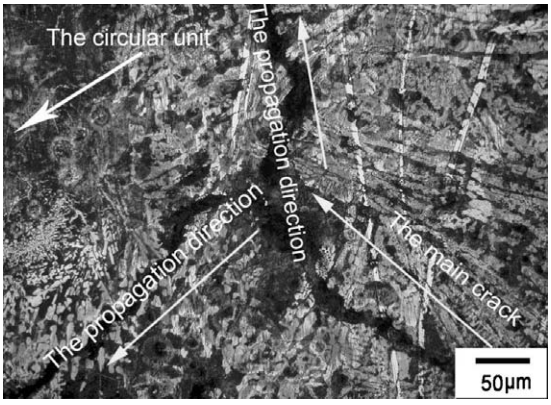

Fig. 10. The propagation of thermal crack hindered by a circular unit.

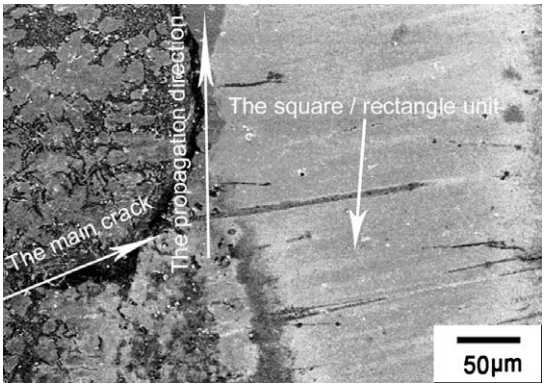

Fig. 11. The propagation of thermal crack hindered by square/rectangle units.

The results as the function of units spacing are presented in Fig. 9. With the increase of the cycles, both the length and the number of main cracks increased. No crack presents at the surface of the sample with the spacing of 2 mm before 600 periods. However, a small amount of micro-cracks were found on the samples with the spacings of 3 mm and 5 mm, respectively. Three 0.5 mm main cracks were initially detected for the sample with the spacing of 2 mm, after 800 fatigue periods. In comparison, four 2 mm and five 2.2 mm main cracks were been found on its counterparts with the spacing of 3 mm and 5 mm respectively. Both the length and the number of main cracks increased with the fatigue period. As for 1600 fatigue periods, the sample with the spacing of 2 mm exhibited eight 4 mm cracks at the surface, and furthermore, the samples with 3 mm and 5 mm spacings have more and bigger cracks, fifteen 4.8 mm cracks and seventeen 5.4 mm ones, respectively. Both the length and number of cracks increase with decreasing the spacing. Apparently, among all the samples tested, the bionic sample with a spacing of 2 mm exhibits the highest crack propagation resistance, in terms of varied spacings.

3.4. The fracture-arrest mechanism of bionic samples with different shapes and varied spacing

Fig. 10 illustrates the propagation route of thermal crack hindered by the circular unit. It shows that, as the crack extended to the circular unit, crack tip got blunt due to high strength and hardness of the inserted H13 steel blocks. The crack suspended there and could not traverse the unit immediately. As we know, the crack propagated around the block and the propagation was only paused temporarily so the resistance to propagation of thermal crack in-

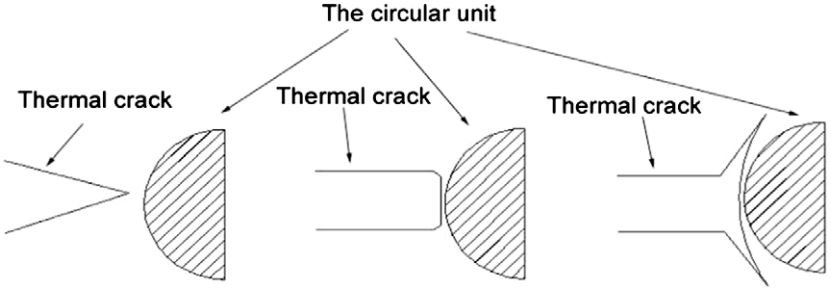

Fig. 12. The model of the hindered crack propagation pattern for circular bionic specimens.

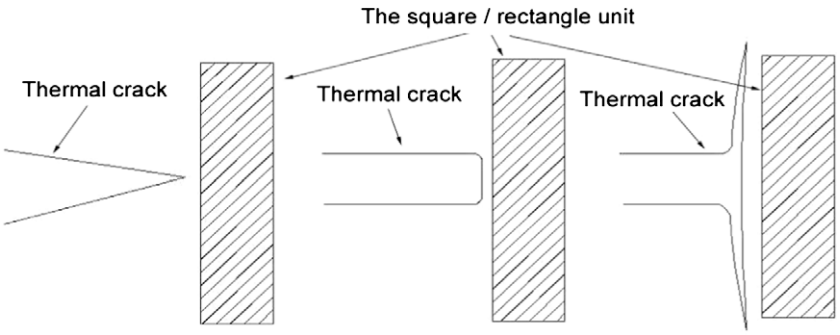

Fig. 13. The model of the hindered crack propagation pattern for square and/or rectangle bionic units.

creases. Fig. 11 shows the propagation pattern of a thermal crack which was hindered by square/rectangular bionic units.

The models of fracture mechanisms and propagation pattern in Figs. 12 and 13 indicate that with the fatigue period increasing, the original orientation of cracks changed, that is, they propagated along the interface of the blocks and matrix, instead of stopping, as mentioned above. In this regard, a far longer fatigue life is obtained, due to the preclusion for the crack propagation. The scenario here coincides with that in the shell nacreous layer, where the cracks could not penetrate the aragonite layer with ease, for they would change its former orientation at the interface of aragonite and organic matter. On the other hand, it is also worth mentioning that the spacing between inserted units. The units induce the change in crack orientation, which made the propagation route very complex. The cracks therefore were precluded between two adjacent units. In view of this fact, smaller spacing would change the crack orientation more frequently, as it progressed between the two units. This mechanism has given the sample a longer fatigue life.

4. Conclusion

In view of the microstructure analysis, micro-hardness measurements and the thermal fatigue resistance comparisons for the bionic samples used in this study, we give the following conclusions:

(1) A bionic structure, with similar structure to alternately soft-and-hard structured nacreous layers, is formed between the matrix and inserted H13 steel blocks. A sound metallurgical bonding exists at the interface of H13 units and vermicular cast iron. The surface microstructure on a bionic unit consists of the inserted H13 steel blocks, a transition zone, interface and the matrix.
(2) The average micro-hardness of the bionic samples varies from HV 500 to HV 760, which is much higher than that of matrix (HV 400). It shows that the cast-in process enhances markedly micro-hardness of units.
(3) The thermal fatigue test shows that the bionic structure has a beneficial effect on improving thermal fatigue resistance of vermicular cast iron, and moreover the bionic samples with the circular cross section exhibits the highest wear resistance. Among all the samples, those with spacing of 2 mm have a far longer thermal fatigue life.
(4) Due to the bionic structure, the thermal fatigue crack is unable to penetrate samples with ease, and expands at the interface of H13 blocks and the matrix, which markedly prolongs thermal fatigue life.

Acknowledgements

This article was supported by the Project 985-Automotive Engineering of Jilin University, the National Natural Science Fund of China (No. 50635030) and the Science and Development Foundation of Jilin (No. 20060196) for financial support.

References

[1] Yamabe J, Takagi M, Matsui T, Kimura T, Sasaki M. Development of disc brake rotors for trucks with high thermal fatigue strength. JSAE Rev 2002;23:105–12.
[2] Yamazaki T, Shibuya T, Jin CJ, Kikuta T, Nakatani N. Lining of hydraulic cylinder made of cast iron with copper alloy. J Mater Process Technol 2006;172:30–4.
[3] Pye AM. Applications of some of the newer cast irons. Mater Design 1982;3(4):534–7.
[4] Çetinkaya C. An investigation of the wear behaviours of white cast irons under different compositions. Mater Design 2006;27(6):437–45.
[5] Cueva G, Sinatora A, Guesser WL, Tschiptschin AP. Wear resistance of cast irons used in brake disc rotors. Wear 2003;255:1256–60.
[6] Daimaruya M, Kobayashi H, Fuad K. Thermoelasto-plastic stresses and thermal distortions in a brake drum. J Therm Stresses 1997;20:345–61.
[7] Thomas JM, Steven CN, Ball KJ, Bedell BC, Bim-Merle DP. Thermal cracking in disc brakes. Eng Fail Anal 2002;9:63–76.
[8] Malak NJ, Al-Nimr M. Dynamic thermal behavior of a brake system. Int Commun Heat Mass Transfer 2001;28:835–45.
[9] Hadavi SMM, Abdollah-Zadeh A, Jamshidi MS. The effect of thermal fatigue on the hardness of hard chromium electroplatings. J Mater Process Technol 2004;147:385–8.
[10] Campos MF, Lopes L, Magina P, Tavares F. Texture and microtexture studies in different types of cast irons. Mater Sci Eng A 2005;398:164–70.
[11] Zhang Y, Chen Y, He R, Shen B. Investigation of tribological properties of brake shoe materials-phosphorous cast irons with different graphite morphologies. Wear 1993;166:179–86.
[12] Shen B, Chen Y, Zhang Y, Zhang Y, Chin. Tribological properties of compacted graphite cast iron bearing vanadium under dry sliding. J Iron Steel Res 1997;9:47–50.
[13] Cheng HF, Huang XM, Chen YQ, Su Y. Failure analysis of HT 200 wear brake drum and improvement of its material. Mater Mech Eng 2001;25:36–8.
[14] Zhou H, Tong X, Zhang ZH, Li XZ, Ren LQ. The thermal fatigue resistance of cast iron with biomimetic non-smooth surface processed by laser with different parameters. Mater Sci Eng A 2006;428:141–7.
[15] Tong X, Zhou H, Zhang W, Zhang ZH, Ren LQ. Thermal fatigue behavior of gray cast iron with striated biomimetic non-smooth surface. J Mater Process Technol 2008;206:473–80.
[16] Tong X, Zhou H, Zhang ZH, Sun N, Shan HY, Ren LQ. Effects of surface shape on thermal fatigue resistance of biomimetic non-smooth cast iron. Mater Sci Eng A 2007;467:97–103.